DOI: https://10.83080/rejost.vol6no3.289

Researchers Journal of Science and Technology (REJOST)

https://rejost.com.ng

Geomechanical Characterization of Elastic and Strength Properties in X Field, Niger Delta, Nigeria

Olomoh Abdulraheem Abdulkadir[1]*, Egbeyale Godwin Babatunde[1], Omolaiye Gabriel Efomeh[2]

Abstract

The study presents a comparative geomechanical characterization of four wells (A–D) in an onshore Niger Delta field using conventional wireline logs. Gamma ray, density, compressional sonic, shear sonic, resistivity, and caliper logs were integrated to estimate Poisson's ratio, static and dynamic Young's modulus, uniaxial compressive strength (UCS), cohesion, friction angle, and Mohr–Coulomb failure strength using established rock physics and empirical relationships. Well correlation identified two laterally continuous reservoir units (Sand 1 and Sand 2), although reservoir thickness varies across the field. The estimated geomechanical properties reveal clear lithological variations in formation mechanical behaviour. Poisson's ratio ranges from approximately 0.29 to 0.43, static Young's modulus from approximately 5 to 19 GPa, dynamic Young's modulus from approximately 23 to 50 GPa, UCS from approximately 860 to 3,780 psi, cohesion from approximately 285 to 980 psi, friction angle from approximately 23° to 35°, and Mohr–Coulomb failure strength from approximately 626 to 4,462 psi. Sandstone intervals generally exhibit lower Poisson's ratio and higher elastic stiffness, compressive strength, cohesion, friction angle, and failure strength than adjacent shale units, indicating greater mechanical competence. Comparative analysis indicates that Well C records the highest maximum values for several elastic and strength parameters, whereas Well B generally exhibits comparatively weaker and more deformable formation intervals. The study provides a field-specific evaluation of the spatial variability of log-derived elastic and strength properties and establishes a comparative basis for reservoir characterization and future geomechanical investigations in the onshore Niger Delta.

✉ Olomoh, Abdulraheem Abdulkadir: abdulraheemabdulkadiro@gmail.com; Phone: +234 703 029 7648

[1] Department of Physics and Materials Science, Kwara State University, Malete, Kwara State, Nigeria

[2] Department of Geology and Mineral Science, Kwara State University, Malete, Kwara State, Nigeria

Keywords: Young's Modulus; Poisson's Ratio; Mohr–Coulomb Failure Criterion; Niger Delta; Cohesion; Friction Angle

Article history

Received: April 17, 2026
Received in revised form: June 21, 2026
Accepted for publication: July 10, 2026
Available online: August 13, 2026

1.0 Introduction

Geomechanical elastic and inelastic properties are fundamental parameters for understanding rock behaviour and ensuring wellbore stability during drilling. The oil and gas industry reportedly spends about $10 billion annually on borehole instability - related problems, highlighting the importance of reliable geomechanical characterization. Elastic properties describe the response of rocks to applied stress and include parameters such as Young's modulus and Poisson's ratio, while strength properties define the resistance of rocks to failure and include parameters such as uniaxial compressive strength, cohesion, and friction angle (Akpan et al., 2021). Exceeding the strength limit of a formation may result in deformation, rock failure, and wellbore instability. Therefore, accurate characterization of rock elastic and strength properties is essential for understanding formation mechanical behaviour and supporting safe and efficient drilling operations (Abijah & Tse, 2016; Ogbuagu *et al*., 2025).

The Niger Delta Basin is one of Africa's most prolific hydrocarbon provinces, consisting predominantly of thick clastic sedimentary sequences characterized by considerable lithological heterogeneity. Variations in sandstone and shale distribution, burial history, compaction, and diagenesis result in significant spatial differences in the mechanical behaviour of reservoir formations. Understanding these variations is important for reservoir characterization (George, 2021; Horsfall *et al*., 2024), and for evaluating the mechanical competence of formations across producing fields. Recent studies have demonstrated the usefulness of geomechanical analyses for characterizing reservoir formations and supporting subsurface evaluation in the Niger Delta (Lawson-Jack *et al*., 2019; Akpan *et al*., 2022 a, b; Ogbuagu *et al*., 2025).

Rock mechanical properties such as Young's modulus, Poisson's ratio, uniaxial compressive strength (UCS), cohesion, and internal friction angle are widely used to describe the elastic and strength characteristics of geological formations. Young's modulus quantifies rock stiffness, whereas Poisson's ratio describes the relationship between axial and lateral deformation under applied stress (Davarpanah *et al*., 2020). Cohesion and internal friction angle govern the shear strength behaviour of rocks and form the basis of the Mohr–Coulomb failure criterion, which is commonly used in geomechanical studies to evaluate the relative mechanical competence of subsurface formations. The combined interpretation of these parameters provides valuable insight into lithology - dependent variations in rock mechanical behaviour (Chang *et al*., 2006; Aadnøy & Looyeh, 2019; Udosen et al., 2018, 2024a, b).

Although laboratory testing of core samples provides direct measurements of rock mechanical properties, continuous core recovery is often expensive and unavailable over the entire depth interval of a well. Consequently, conventional wireline logs have become one of the most widely used data sources for estimating elastic and strength parameters through empirical rock physics relationships. Advances in well-log interpretation have enabled the estimation of dynamic and static elastic properties, as well as strength parameters, allowing continuous, depth-dependent geomechanical characterization of reservoir intervals (Ogbuagu *et al*., 2025).

Therefore, this study presents a comparative geomechanical characterization of four wells in an onshore Niger Delta field using conventional wireline logs. Conventional wireline logs, including gamma ray, density, compressional sonic, shear sonic, resistivity, and caliper logs, were used to estimate Poisson's ratio, static and dynamic Young's modulus, uniaxial compressive strength, cohesion, friction angle, and Mohr–Coulomb failure strength using established empirical relationships. The estimated geomechanical parameters were subsequently compared to evaluate lithology-dependent variations in mechanical competence among the studied wells and to provide a field-specific understanding of the spatial variability of rock mechanical properties within the studied onshore Niger Delta reservoirs. No laboratory core measurements or drilling observations were available; therefore, the estimated parameters represent empirical, log-derived estimates rather than direct laboratory measurements.

2.0 Location and Geology of the study area

The X Field is located in the western part of the Niger Delta Basin, between latitudes 4°19′00′N and 5°50′00′N and longitudes 5°30′30′E and 6°10′00′E. Figure 1(a) shows the regional location of the field, while Figure 1(b) shows the spatial distribution of the wells within the study area (Akpan *et al*., 2022). The Niger Delta's stratigraphic succession consists of three main formations that form a thick clastic wedge deposited during the Tertiary in a prograding deltaic setting (Umoh *et al*., 2022, 2025; Ekanem *et al*., 2024). These are the Benin, Agbada, and Akata Formations, in descending stratigraphic order (Short & Stauble, 1967). Knox and Omatsola (1989) noted that their deposition resulted from the dynamic interaction between marine and continental processes, strongly influenced by deltaic progradation and relative sea-level variations.

The basin is structurally divided into several depobelts, which served as major sediment transport pathways while also influencing hydrocarbon migration and trap development. The Akata Formation, at the base of the succession, consists primarily of dark marine shales and silty mudstones, with occasional thin turbiditic sandstone interbeds, deposited in a deep-marine setting beginning in the Paleocene. The formation is up to approximately 6 km thick in some locations and is rich in Type II and III organic matter, and is generally recognised as the basin's principal source rock (Murat, 1972). The Agbada Formation constitutes the principal reservoir-bearing unit and consists of alternating sandstones, shales, and siltstones deposited in fluvial, deltaic, and neritic settings (Obianwu *et al*., 2011). This formation, which is up to approximately 4 km thick, ranges from the Eocene to the Pleistocene and contains significant hydrocarbon accumulations, with interbedded shales providing seals and local cap rocks (Doust & Omatsola, 1990). The Benin Formation, the youngest formation, consists predominantly of coarse, weakly cemented continental sands with minor clay intercalations. It reaches thicknesses of up to approximately 1.4 km and was deposited from the Oligocene to the Recent in fluvial and alluvial environments (Tuttle *et al*., 1999; George *et al*., 2022, 2025).

The tectonic evolution of the Niger Delta is strongly related to the rifting of Africa and South America during the Early Cretaceous, followed by post-rift thermal subsidence (Burke, 1972). Deltaic progradation from the Paleocene to the Miocene was characterised by high rates of sediment supply, the development of syndepositional growth faults, and large-scale shale diapirism and rollover structures. These processes resulted in typical rollover anticlines and fault-dependent closures, which contributed to the development of major hydrocarbon traps in the basin (Evamy *et al*., 1978). Within this structural and stratigraphic framework, the X Field benefits from the co-occurrence of mature source rocks associated with the Akata Formation, high-porosity sandstone reservoirs within the Agbada Formation, and a variety of trap types, including fault-bounded closures and growth-related anticlines. These characteristics provide a favourable setting for hydrocarbon accumulation and production in the Niger Delta Basin.

3.0 Material and Methods

3.1 Data Sets

This study utilised quality-checked wireline well log data acquired from hydrocarbon wells in the study region. The dataset included gamma ray, density, compressional sonic, shear sonic, resistivity, and calliper logs that were used to characterise the formations' lithology, petrophysics, and geomechanical properties. Gamma ray logs were used to identify lithologies and estimate shale volume, whilst density logs supplied bulk density data. Compressional and shear sonic logs were utilised to determine elastic characteristics, while resistivity and calliper logs helped with formation appraisal and borehole condition assessment (Ekong *et al.,* 2025).

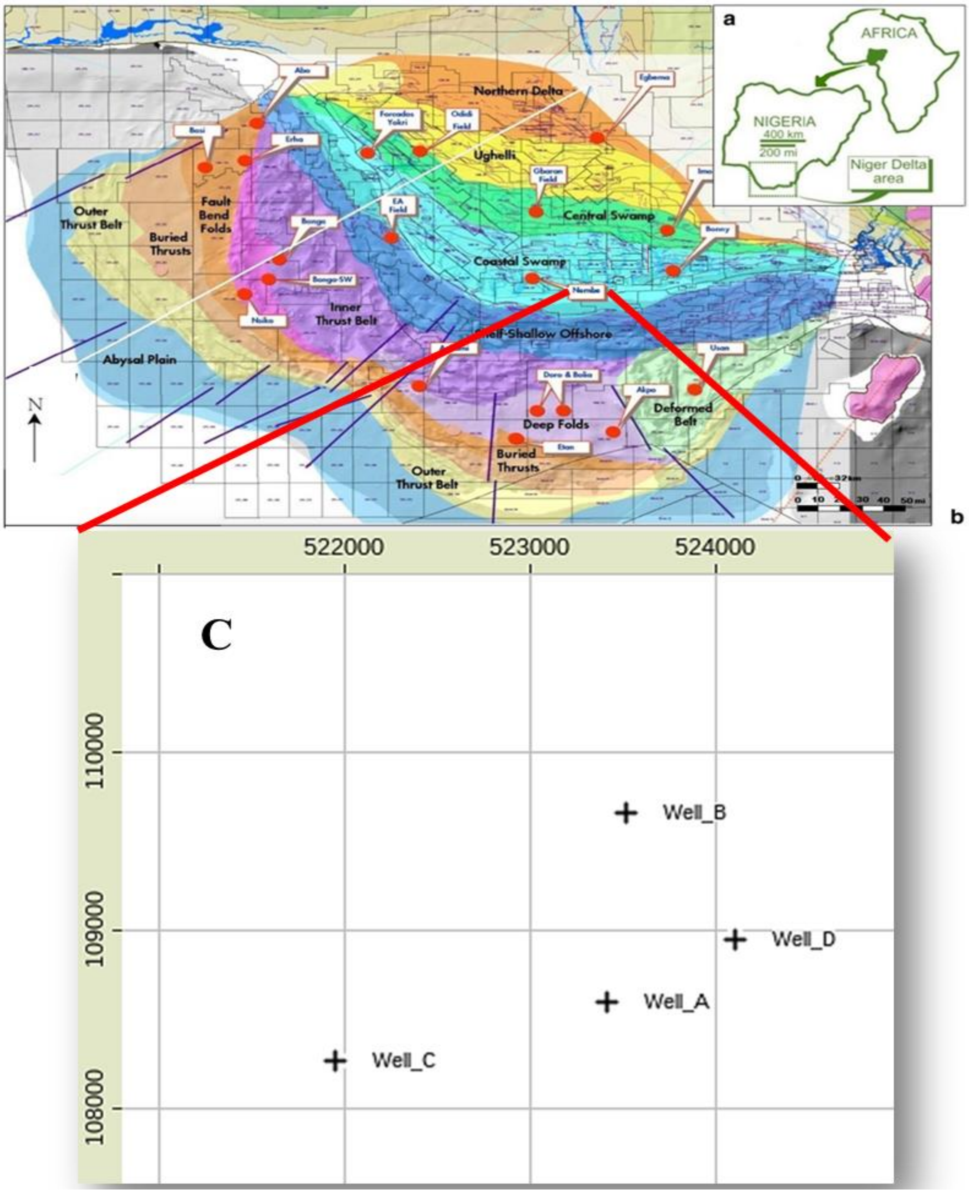

Figure 1: (a) Map of Africa and Nigeria (b) Map showing the location of X field, the study area in the Niger Delta, Nigeria (Ekefre et al., 2025) (c) Base Map Showing Well Distribution in the X field

Following quality control and log conditioning, geomechanical characteristics such as Poisson's ratio, dynamic and static Young's modulus, cohesion, friction angle, and Mohr-Coulomb failure parameters were calculated using recognised rock physics and empirical relationships. These parameters were then utilised to assess the elastic behaviour, strength, and mechanical competency of the reservoir formations (Asquith & Krygowski, 2004; Rider & Kennedy, 2011; Zoback, 2010).

3.2 Well correlation

Well correlation means identifying related lithological boundaries with gamma ray and resistivity logs that are colour-coded for easier distinction. Correlation panels are created using Rokdoc software to evaluate reservoir development. Shale volume is calculated using gamma ray logs and is important in estimating formation porosity, rock quality, and fluid content (Adeoti *et al*., 2009). The volume of shale for Tertiary rock formations is computed using the equation presented by Larionov (1969) in Eq. 1.

$$V_{sh} = 0.083(2^{3.7 I_{GR}} - 1) \quad (1)$$

$$I_{GR} = \frac{GR_{\log} - GR_{\min}}{GR_{\max} - GR_{\min}} \quad (2)$$

where I_{GR} is the Gamma ray index, V_{sh} is volume of shale, $GR_{\log}$ is the GR reading from log, $GR_{\min}$ is the minimum reading of GR log, $GR_{\max}$ is the maximum GR reading.

3.3 1D Geomechanical Model Construction

3.3.1 Poisson's Ratio (ν)

The Poisson's Ratio is an essential parameter that describes how a rock deforms when stressed. This parameter represents the ratio of lateral strain to longitudinal strain (Gercek, 2007). The lesser the Poisson's ratio, the lower the horizontal stress, and the less difficult it is to fracture the rock. A shift in this ratio may suggest a change in the pore fluid (Ebong *et al*., 2023a). The Poisson's ratio can be described in terms of velocity.

$$\nu = \frac{V_P^2 - 2V_S^2}{2(V_P^2 - V_S^2)} \tag{3}$$

3.3.2 Young's Modulus (E)

Y Young's modulus (E) describes the stiffness of a rock and represents the ratio of applied stress to the resulting strain within the elastic range. Higher Young's modulus generally indicates greater rock stiffness, whereas lower values are associated with more compliant formations (Davarpanah *et al*., 2020). In this study, dynamic and static Young's modulus were estimated from the available well-log data using the relationship in Equation (4):

$$E = \rho V_S^2 \left(\frac{2(1+\nu)}{1-2\nu} \right) \tag{4}$$

3.3.3 Uniaxial Compressive Strength (UCS)

Uniaxial Compressive Strength (UCS) represents the maximum axial compressive stress that a rock can withstand under uniaxial loading before failure. In this study, UCS was estimated using Etim *et al*. (2025) relationship (equation 5). This relationship is specifically used for fine grained, consolidated and unconsolidated sandstones with all porosity ranges suitable for the Niger Delta.

$$UCS = 1200^{(-0.036\Delta T_c)} \tag{5}$$

where UCS = Uniaxial Compressive Strength (in psi), Δt_c is the compressional sonic transit time in μs/ft.

3.3.4 Material Strength

The Mohr–Coulomb failure criterion was used to estimate the shear strength of the formation based on cohesion, normal stress, and friction angle. The criterion is expressed as:

$$\tau = C + \sigma_n \tan\phi \tag{6}$$

where τ is the Mohr–Coulomb failure strength (psi), C is cohesion (psi), σ_n is the normal stress (psi), and ϕ is the friction angle (degrees). The normal stress at each depth was taken as the effective vertical stress, computed as the difference between the overburden stress and the estimated pore pressure. Overburden stress was obtained by integrating the density log from surface to total depth, while pore pressure was estimated using Eaton's (1975) method with a sonic-derived exponent of 3. This effective-stress-based normal stress was applied uniformly across all four wells to ensure consistency in the comparative analysis. The criterion was used to evaluate the strength characteristics and relative mechanical competence of the investigated formations (Zoback, 2010; Aadnøy & Looyeh, 2019).

4.0 Results and Discussions

4.1 Well Correlation

Figure 2 illustrates the correlation of Wells A–D based on the interpreted tops and bases of Sand 1 and Sand 2. Both reservoirs exhibit good lateral continuity across the wells, indicating that the sand units are laterally traceable over the study area. However, noticeable variations in reservoir depth and thickness occur between the wells. The tops of both Sand 1 and Sand 2 become progressively shallower from Well A toward Well D, suggesting a structural or stratigraphic elevation change across the field. Sand 1 shows a marked reduction in thickness from 181.13 ft in Well A to 39.34 ft in Well D, while Sand 2 attains its greatest thickness of 299.77 ft in Well B and decreases to 61.83 ft in Well D. The greater thickness observed in Wells A and B indicates more substantial sand development in these locations, whereas the pronounced thinning toward Well D may reflect changes in depositional conditions, facies variation, or progressive reservoir pinch-out. Overall, the combination of good lateral continuity and significant thickness variation indicates a heterogeneous fluvial-deltaic reservoir architecture, with implications for reservoir connectivity, distribution, and volumetric potential (Akpan *et al*., 2022b).

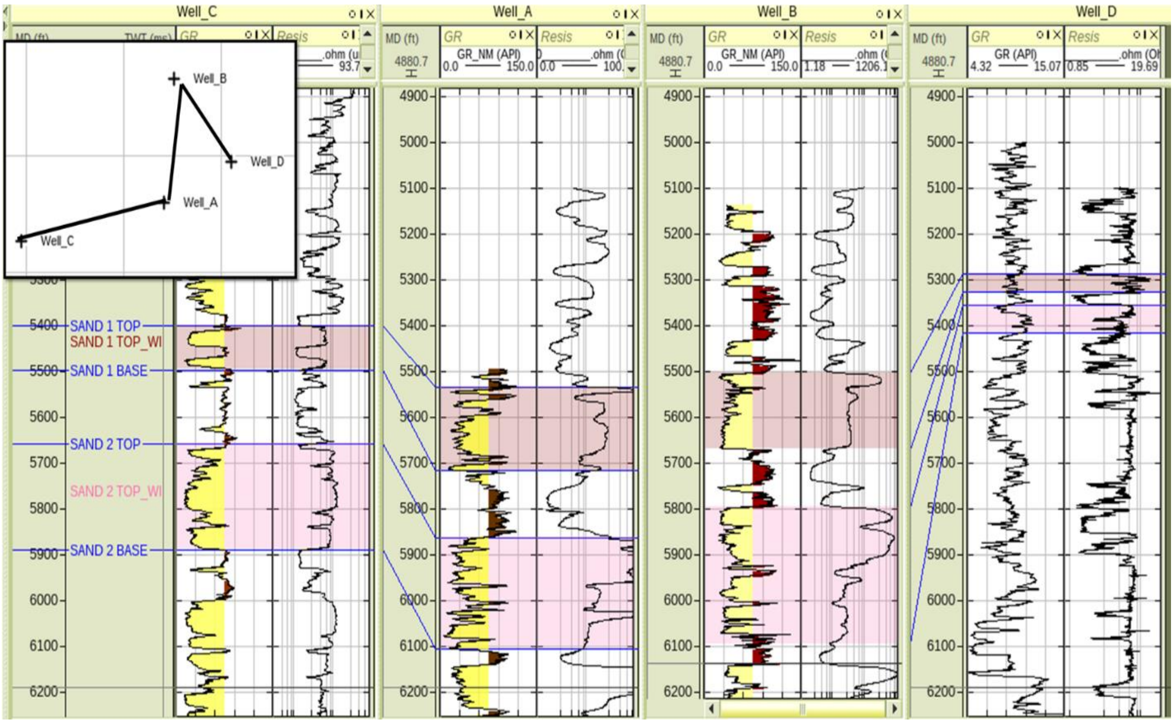

Figure 2.: Well correlation of Well A, Well B Well C and Well D

4.2 Interpretation of the log-derived geomechanical characterization of elastic and strength properties

Figures 3–6 and Tables 1–4 present the log-derived elastic and strength properties estimated for Wells A–D. The results reveal alternating sandstone and shale successions typical of the onshore Niger Delta, with pronounced vertical and lateral variations in mechanical properties. These variations are closely related to lithology and burial depth, with sandstone intervals consistently exhibiting greater stiffness and strength than the adjacent shale units. The higher mechanical competence of the sandstone intervals is reflected by their relatively lower Poisson's ratio, higher Young's modulus, greater uniaxial compressive strength (UCS), higher cohesion, larger friction angles, and greater Mohr–Coulomb failure strength (Lamorde *et al*., 2014).

The estimated Poisson's ratio varies from approximately 0.30–0.41 in Well A, 0.32–0.43 in Well B, 0.29–0.42 in Well C, and 0.35–0.42 in Well D. In all four wells, higher Poisson's ratio values are predominantly associated with shale intervals, indicating relatively ductile behaviour and a greater tendency for lateral deformation under stress. Conversely, the lower values observed within sandstone intervals reflect increased rock stiffness and reduced deformability, a characteristic commonly associated with quartz-rich clastic reservoirs.

The estimated elastic moduli exhibit an overall increase with depth despite local fluctuations associated with interbedded lithologies. The static Young's modulus reaches values of approximately 19 GPa in Well A, 12 GPa in Well B, 19 GPa in Well C, and 11 GPa in Well D, whereas the dynamic Young's modulus exceeds 50 GPa in Wells A and C and attains approximately 38 GPa and 37 GPa in Wells B and D, respectively. The consistently higher dynamic modulus relative to the static modulus reflects the difference between small-strain elastic wave measurements and larger-strain rock deformation represented by static behaviour. The overall increase in elastic stiffness with depth is attributed to progressive compaction, porosity reduction, and diagenetic cementation, which enhance the rigidity of sedimentary rocks (Fjaer *et al*., 2021).

The estimated uniaxial compressive strength follows a similar trend, with stronger sandstone intervals consistently corresponding to zones of higher elastic stiffness. Maximum UCS values reach approximately 3,406 psi in Well A, 2,884 psi in Well B, 4,968 psi in Well C, and 2,176 psi in Well D. The comparatively lower maximum recorded in Well D reflects gaps in the available log data for this well. Conversely, the lower UCS values observed within shale-rich intervals indicate comparatively weaker formations that are more susceptible to compressive deformation. The positive relationship between Young's modulus and UCS suggests that the mechanically stiffer formations also possess greater resistance to compressive failure (Rybacki *et al*., 2015).

The estimated shear strength parameters further differentiate the mechanical behaviour of the studied formations. Cohesion ranges from approximately 372–889 psi in Well A, 285–780 psi in Well B, 328–1,149 psi in Well C, and 331–614 psi in Well D. Similarly, the friction angle ranges from 25.6°–34.3° in Well A, 22.9°–33.1° in Well B, 24.5°–35.3° in Well C, and 24.5°–30.7° in Well D, with the higher values occurring predominantly within sandstone intervals. As with UCS, the narrower ranges recorded in Well D are attributable to incomplete log coverage in this well rather than a true absence of high-strength intervals. The combined increase in cohesion and friction angle results in improved shear resistance, consistent with the Mohr–Coulomb failure criterion (Zoback, 2010).

The estimated Mohr–Coulomb failure strength exhibits a comparable pattern across the four wells. Values range from approximately 1,472–4,250 psi in Well A, 626–2,589 psi in Well B, 1,431–4,462 psi in Well C, and 1,407–2,635 psi in Well D. Higher failure strengths are concentrated within the deeper sandstone intervals, where the combined effects of greater elastic stiffness, higher cohesion, and larger friction angles provide increased resistance to shear failure. In contrast, the shale-rich intervals consistently record lower failure strengths, reflecting their comparatively weaker mechanical behaviour.

Comparison of the four wells reveals distinct differences in their geomechanical characteristics. Well C records the highest maximum values for static and dynamic Young's modulus, UCS, cohesion, friction angle, and Mohr–Coulomb failure strength, indicating the presence of the most mechanically competent intervals in the field. Well A also contains highly competent intervals and records the second-highest maximum Mohr–Coulomb failure strength (4,250 psi). Well B generally records the lowest elastic stiffness, strength, and cohesion values, together with the highest maximum Poisson's ratio, indicating comparatively weaker and more deformable formations. Well D exhibits intermediate-to-low maximum strength values; this is interpreted with caution, however, as gaps in the available log data limited the depth range and completeness of the Well D dataset relative to Wells A, B, and C.

The elastic and strength properties demonstrate that lithology is the principal control on the estimated mechanical behaviour of the investigated formations. Sandstone intervals generally exhibit greater stiffness, compressive strength, and shear resistance than adjacent shale units, while the general increase in mechanical properties with depth reflects progressive burial, compaction, and diagenetic cementation typical of the onshore Niger Delta (Fjaer *et al*., 2021). Although the reported properties were derived from empirical log-based correlations rather than direct laboratory measurements or complete in-situ stress analyses, they provide a useful comparative assessment of formation mechanical behaviour and a dataset for future geomechanical investigations within the study area.

.

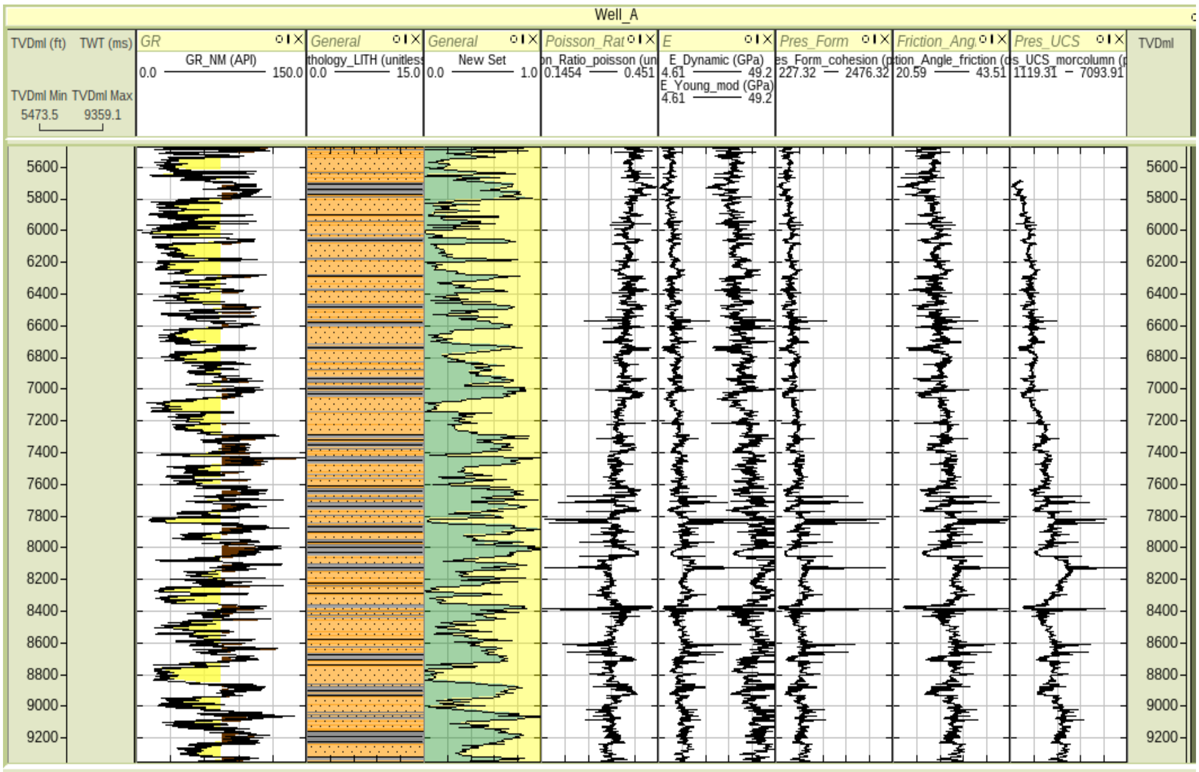

Figure 3: Log Display of 1D MEM. Gamma Ray (Track 1), Lithology log (Track 2), Volume of Shale (Track 3), Poisson's Ratio (Track 4), Young's Modulus: Static and Dynamic (Track 5), Cohesion (Track 6), Friction Angle (Track 7), Mohr-Coulomb failure criterion (Track 8) (From Left to Right Panel) for Well A

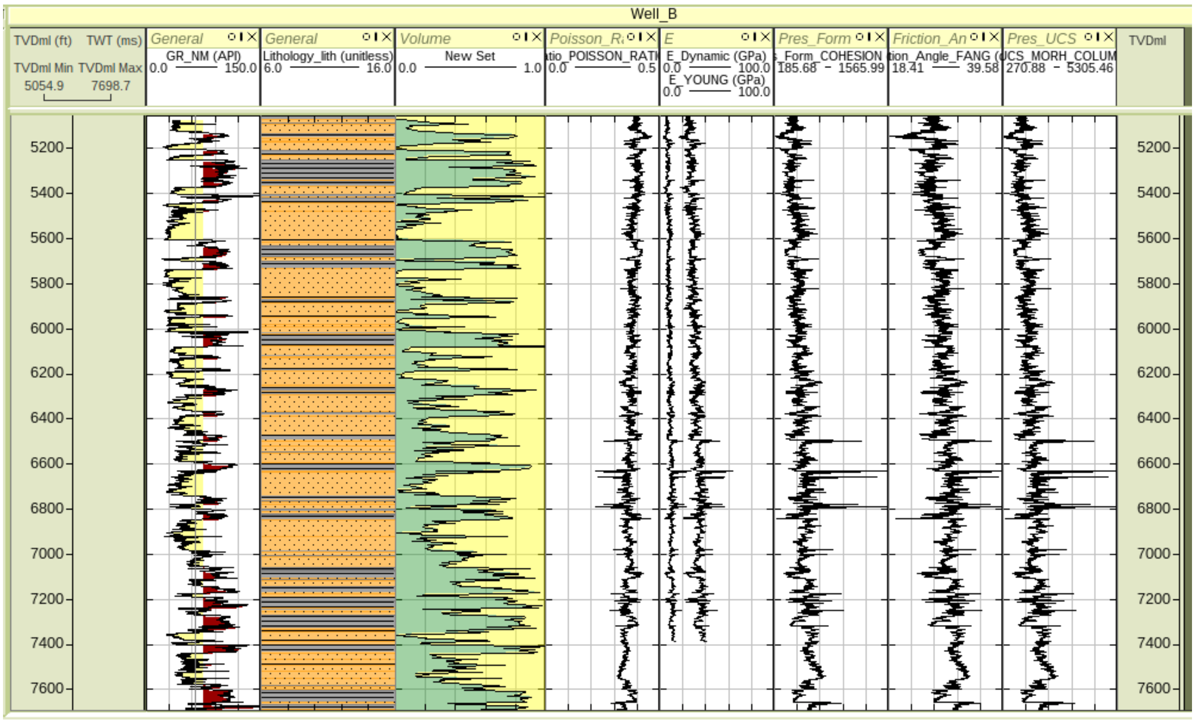

Figure 4: Log Display of 1D MEM. Gamma Ray (Track 1), Lithology log (Track 2), Volume of Shale (Track 3), Poisson's Ratio (Track 4), Young's Modulus: Static and Dynamic (Track 5), Cohesion (Track 6), Friction Angle (Track 7), Mohr-Coulomb failure criterion (Track 8) (From Left to Right Panel) for Well B.

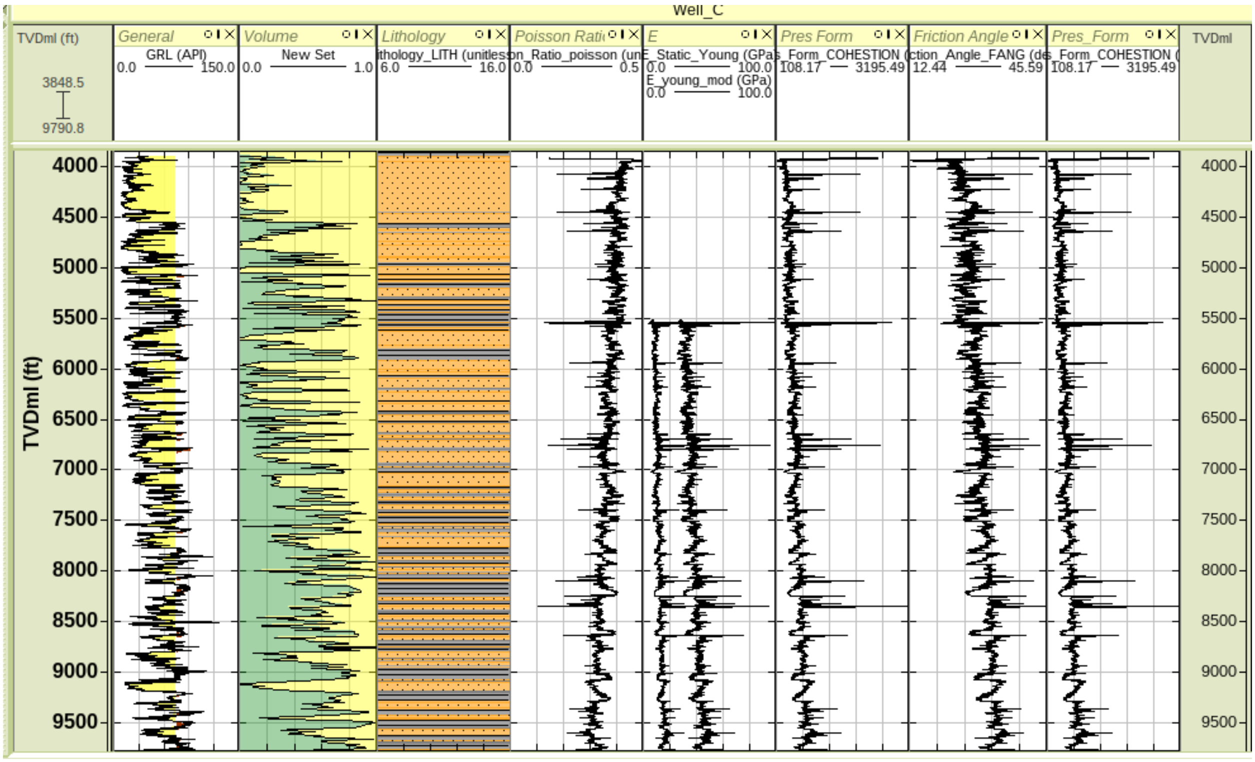

Figure 5: Log Display of 1D MEM. Gamma Ray (Track 1), Lithology log (Track 2), Volume of Shale (Track 3), Poisson's Ratio (Track 4), Young's Modulus: Static and Dynamic (Track 5), Cohesion (Track 6), Friction Angle (Track 7), Mohr-Coulomb failure criterion (Track 8) (From Left to Right Panel) for Well C.

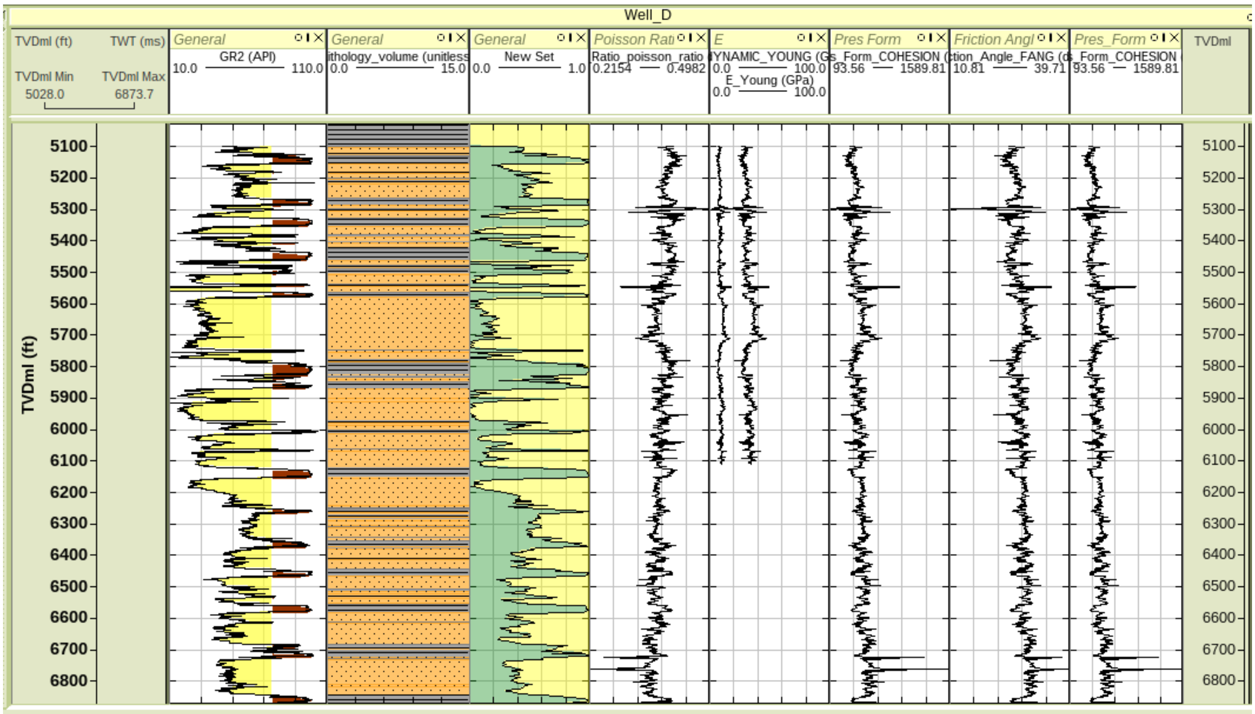

Figure 6: Log Display of 1D MEM. Gamma Ray (Track 1), Lithology log (Track 2), Volume of Shale (Track 3), Poisson's Ratio (Track 4), Young's Modulus: Static and Dynamic (Track 5), Cohesion (Track 6), Friction Angle (Track 7), Mohr-Coulomb failure criterion (Track 8) (From Left to Right Panel) for Well D.

Table 1: Summary of Geomechanical Parameters by Lithology for Well A

Measured Depth (ft)	Rock Type (Lithology)	Poisson's Ratio	Dynamic Young Modulus (GPa)	Static Young Modulus (GPa)	Uniaxial Compressive Strength (Psi)	Cohesion Strength (Psi)	Friction Angle (Degrees)	Mohr-Coulomb failure criterion (Psi)
5757.50	Sand	0.3865	9.1295	32.5565	1464.3549	443.3449	27.5449	1633.3477
5861.50	Shale	0.4060	8.0169	29.9452	1190.9828	372.3283	25.6270	1472.2081
6111.50	Sand	0.3731	9.4601	33.2254	1693.8949	500.1017	28.7130	1911.4290
6141.50	Shale	0.3880	9.8112	33.9621	1443.7535	437.9218	27.3933	1859.0859
6238.50	Sand	0.3700	9.7168	33.8152	1741.8166	512.2782	29.0008	2052.3557
6252.00	Shale	0.3824	10.8080	36.1070	1531.5303	460.1528	27.9131	1980.0435
6340.00	Sand	0.3564	11.2833	37.0516	1999.6086	574.5931	30.1313	2286.7855
6355.00	Shale	0.3776	11.4706	37.3659	1628.3873	483.2870	28.2946	2086.4281
6427.50	Sand	0.3749	9.4847	33.2938	1660.8496	492.0832	28.5632	2101.3067
6448.00	Shale	0.3959	8.8816	31.8666	1340.4298	410.5723	26.5969	1891.7603
6523.50	Sand	0.3686	10.2765	34.9489	1773.7091	519.6956	29.1029	2166.2517
6556.00	Shale	0.3959	8.9797	32.1694	1327.9288	408.2018	26.6448	1888.4349
6643.00	Sand	0.3645	10.6745	35.6947	1868.9745	541.7231	29.4274	2236.8357
6670.00	Shale	0.3740	11.4382	37.3239	1685.2638	497.6271	28.6194	2136.6769
6780.00	Sand	0.3574	11.2327	36.8949	1991.7807	572.1106	30.0359	2283.6445
6814.50	Shale	0.3932	9.1361	32.4416	1377.4285	420.2399	26.8545	1892.3530
6990.00	Sand	0.3579	11.1159	36.7143	1973.3506	568.1981	30.0083	2245.8165
7024.00	Shale	0.3786	10.7836	35.9891	1615.8035	479.9256	28.1903	2032.4095
7045.50	Sand	0.3604	10.8119	36.1151	1918.4414	555.2875	29.8117	2199.5158
7117.50	Shale	0.3799	10.6454	35.6367	1609.9003	477.3669	28.0427	1987.9447
7348.00	Sand	0.3482	11.2560	36.9592	2168.4614	614.7481	30.7944	2557.7453
7386.50	Shale	0.3491	13.4892	41.3260	2165.8105	613.1360	30.6920	2831.8911
7401.50	Sand	0.3467	13.5972	41.6214	2193.8073	621.0603	30.9271	2824.8561
7465.50	Shale	0.3702	11.2152	36.9166	1749.8251	513.6257	28.9630	2512.1824
7484.50	Sand	0.3320	13.7039	41.8057	2521.5394	697.4654	32.0609	3027.8139
7538.50	Shale	0.3427	12.6608	39.7956	2288.7618	642.8581	31.2200	2904.4288
7684.50	Sand	0.3380	12.4482	39.3605	2389.1179	666.4755	31.5913	2901.2721

7760.50	Shale	0.3614	12.1260	38.6320	1976.6447	564.8198	29.6090	2647.2142
7778.00	Sand	0.3172	15.1088	43.8482	3147.2608	826.0450	32.9244	3248.2717
7828.50	Shale	0.3655	11.9545	38.3072	1846.0803	536.4386	29.3299	2692.6332
7921.50	Sand	0.3086	17.4414	47.5779	3382.0829	877.3009	33.6085	3580.1537
7972.00	Shale	0.3409	14.5269	43.2699	2340.5288	654.4133	31.3507	3189.4696
8011.50	Sand	0.3304	13.9393	42.1959	2578.4162	709.5545	32.1630	3347.4468
8118.00	Shale	0.3607	13.1986	40.6062	1986.4112	567.4790	29.6615	2898.4872
8153.00	Sand	0.3183	14.9279	43.9259	2908.5450	783.3028	33.0345	3723.4287
8208.00	Shale	0.3036	18.6396	50.1345	3406.3820	888.7092	34.0490	4250.4085
8419.00	Sand	0.3209	14.7318	43.6703	2803.4500	761.3489	32.8732	3565.3699
8448.50	Shale	0.3691	13.0821	39.1223	2179.1392	591.2817	28.4307	2566.3957
8635.50	Sand	0.3367	12.9100	40.2748	2424.2936	674.4353	31.6903	3004.0383
8643.50	Shale	0.3194	15.3767	44.8976	2832.7471	768.5264	33.0000	3352.4280
8684.50	Sand	0.3072	17.2128	47.7206	3281.2199	862.5840	33.7857	3583.9008
8698.50	Shale	0.3229	15.1437	44.4645	2748.6575	749.2116	32.7369	3403.0570
8736.50	Sand	0.3153	16.2179	46.0976	3023.3622	807.0160	33.2263	3528.4475
8778.00	Shale	0.3619	12.8947	40.1483	1926.4953	555.0443	29.6234	2858.6344
8917.50	Sand	0.3258	11.9927	38.4214	2688.4885	734.8829	32.5088	3320.8274
9001.00	Shale	0.3558	13.1996	40.6839	2051.1774	584.7877	30.1145	2961.8300
9095.50	Sand	0.3270	13.0364	40.5164	2657.5576	727.8680	32.4200	3567.2568
9149.50	Shale	0.3199	15.5253	45.1106	2839.7649	769.0395	32.9371	3868.3730
9200.00	Sand	0.3255	14.1831	42.6472	2688.9414	735.3284	32.5391	3828.1725
9299.00	Shale	0.3322	14.2418	42.8036	2525.2545	697.8716	32.0315	3662.1421
9381.00	Sand	0.3150	14.6533	43.5164	2951.2638	795.0722	33.3149	3859.2567
9401.00	Shale	0.3385	13.5302	41.4347	2396.7568	667.3626	31.5325	3510.8606
9437.50	Sand	0.3096	15.1802	44.5117	3095.9982	827.4629	33.6979	3906.3690
9505.50	Shale	0.3418	14.0430	42.3942	2317.8742	649.1907	31.2805	3337.6745
9620.00	Sand	0.3089	16.2776	46.4658	3118.9376	832.4451	33.7481	3734.8184
9634.50	Shale	0.3100	18.0148	49.4797	3093.9627	826.6431	33.6685	3749.5579
9711.00	Sand	0.3014	15.6574	45.3418	3330.4595	879.4143	34.2805	3880.6905
9812.50	Shale	0.3455	14.3752	42.9285	2258.0990	634.0853	30.9608	3166.9577

Table 2: Summary of Geomechanical Parameters by Lithology for Well B

Measured Depth (ft)	Rock Type (Lithology)	Poisson's Ratio	Dynamic Young Modulus (GPa)	Static Young Modulus (GPa)	Uniaxial Compressive Strength (Psi)	Cohesion Strength (Psi)	Friction Angle (Degrees)	Mohr-Coulomb failure criterion (Psi)
5136.00	Shale	0.4079	5.4605	23.6056	1169.1380	366.3014	25.3736	949.1497
5196.00	Sand	0.3951	6.2955	25.8342	1340.3875	411.3409	26.7133	1127.1174
5217.00	Shale	0.4316	5.0485	22.5582	863.5717	285.2794	22.9280	626.0400
5271.00	Sand	0.3859	7.4996	28.7114	1491.6424	449.1718	27.5406	1280.5751
5291.50	Shale	0.4140	6.0667	25.3047	1074.5822	342.3316	24.8540	849.0631
5314.50	Sand	0.3879	6.8410	27.1811	1454.8602	440.2013	27.3804	1243.3636
5432.00	Shale	0.4042	6.8791	27.2812	1208.7355	377.4061	25.8375	989.9096
5467.50	Sand	0.4052	5.5642	23.8608	1193.6067	373.5640	25.7420	974.4703
5504.50	Shale	0.3984	7.3073	28.2921	1295.4426	399.6184	26.3944	1079.6861
5701.50	Sand	0.3810	7.6819	29.1672	1565.6324	468.0301	28.0083	1356.1559
5747.50	Shale	0.4095	6.8612	27.2841	1134.4231	358.1236	25.3178	912.2266
5763.50	Sand	0.3701	8.5495	31.0619	1777.6190	518.9258	28.9037	1559.3372
5796.50	Shale	0.4006	7.2046	28.1226	1253.2428	389.3485	26.2120	1037.5774
5935.00	Sand	0.3792	7.3698	28.4691	1590.9664	474.5754	28.1766	1382.6352
5947.00	Shale	0.3923	8.7023	31.5822	1375.2871	420.6893	27.0028	1164.6907
6083.50	Sand	0.3802	7.8624	29.6073	1572.5043	470.0979	28.0950	1364.6319
6141.00	Shale	0.3829	8.2774	30.5958	1528.6017	459.0660	27.8453	1320.1956
6325.50	Sand	0.3705	8.7271	31.5842	1748.8485	513.0858	28.9190	1537.3633
6357.50	Shale	0.3778	9.3972	33.0359	1622.6483	481.9584	28.2747	1412.2556
6435.00	Sand	0.3701	8.8402	31.8525	1749.5083	513.6369	28.9705	1539.9508
6449.00	Shale	0.3976	7.5791	28.9982	1297.9864	400.7751	26.4892	1084.0382
6534.00	Sand	0.3706	8.9917	32.2152	1736.5442	510.6864	28.9361	1528.2014
6560.00	Shale	0.4004	7.1021	27.8327	1259.2040	390.6852	26.2197	1043.3086
6661.00	Sand	0.3622	9.9839	34.3351	1908.1148	551.4031	29.6311	1688.8979
6693.50	Shale	0.3766	9.5867	33.4616	1635.6441	485.5939	28.4003	1426.9014
6808.50	Sand	0.3498	11.0804	36.5036	2181.7129	615.0352	30.6109	1936.6429

6831.50	Shale	0.3809	9.1107	32.3666	1577.3488	470.3261	27.9900	1364.7147
6863.50	Sand	0.3410	12.0226	38.2816	2439.8273	671.7864	31.2227	2148.7217
6873.00	Shale	0.3612	9.9052	34.2279	1903.5419	551.6628	29.7434	1693.3463
6884.00	Sand	0.3561	11.1591	36.8283	2004.8050	575.9350	30.1629	1791.1738
6910.00	Shale	0.3927	8.3691	30.7521	1389.9387	423.0980	26.8831	1175.2033
7130.00	Sand	0.3626	9.7288	33.8019	1887.3005	547.1936	29.6121	1674.3672
7181.00	Shale	0.3770	8.8277	31.5824	1659.3967	489.7512	28.2850	1442.9802
7207.00	Sand	0.3485	10.8185	36.1458	2152.8931	611.4721	30.7814	1934.2124
7236.00	Shale	0.3635	10.4579	35.3385	1874.3861	543.7951	29.5154	1661.3352
7254.50	Sand	0.3404	11.9466	38.3970	2347.5869	656.1940	31.3956	2107.7109
7301.50	Shale	0.3640	9.4417	32.9668	1886.7740	545.6452	29.4339	1666.7236
7334.50	Sand	0.3460	11.7523	37.9170	2235.2085	629.3783	30.9462	2000.4251
7392.50	Shale	0.3801	9.2682	32.7977	1587.8169	473.0880	28.0771	1375.4478
7468.00	Sand	0.3438	N/A	37.3373	2257.5730	635.9701	31.1517	2029.8656
7501.00	Shale	0.3563	N/A	N/A	1997.9722	574.4347	30.1506	1784.9593
7665.50	Sand	0.3487	N/A	N/A	2155.5578	611.7659	30.7552	1933.3610
7721.00	Shale	0.3821	N/A	N/A	1539.8412	461.9576	27.9276	1331.5279
7773.00	Sand	0.3402	N/A	N/A	2366.3994	659.7610	31.3968	2119.4319
7825.50	Shale	0.3643	N/A	N/A	1861.7859	540.6057	29.4453	1648.0328
7936.00	Sand	0.3233	N/A	N/A	2737.7880	746.7921	32.7096	2462.3364
7982.00	Shale	0.3177	N/A	N/A	2883.5868	779.6639	33.1156	2589.2923

Table 3: Summary of Geomechanical Parameters by Lithology for Well C

Measured Depth (ft)	Rock Type (Lithology)	Poisson's Ratio	Dynamic Young Modulus (GPa)	Static Young Modulus (GPa)	Uniaxial Compressive Strength (Psi)	Cohesion Strength (Psi)	Friction Angle (Degrees)	Mohr-Coulomb failure criterion (Psi)
5622.50	Shale	0.41809	26.96124	6.72543	1018.323	327.6821	9.42823	1430.505
5632.00	Sand	0.30742	49.10667	20.16160	4968.409	1148.586	22.6531	2830.581
5668.00	Shale	0.39069	31.62755	8.81357	1437.719	434.1156	12.62748	1789.263
5889.50	Sand	0.37426	32.70118	9.21493	1672.138	494.8516	14.56484	2023.573
6000.00	Shale	0.39786	30.35893	8.18485	1307.895	402.4948	11.78739	1649.81
6275.50	Sand	0.36997	33.48681	9.59790	1761.941	516.0088	15.07357	2166.367
6304.00	Shale	0.39355	32.14415	8.94852	1355.834	415.7678	12.29179	1976.471
6401.50	Sand	0.35604	36.30607	10.90206	2002.318	575.5083	16.73393	2450.1
6417.00	Shale	0.37597	35.03125	10.30252	1638.805	486.8389	14.36277	2201.182
6503.50	Sand	0.37122	33.13868	9.41296	1727.463	508.3606	14.92591	2172.973
6534.00	Shale	0.38084	34.05043	9.84121	1562.129	467.4819	13.78751	2002.418
6606.50	Sand	0.36766	33.90842	9.75607	1783.837	522.5681	15.34752	2144.007
6627.00	Shale	0.40021	29.40855	7.75223	1261.326	391.298	11.51274	1793.147
6712.00	Sand	0.37120	32.96636	9.32401	1719.41	506.8448	14.92733	2105.719
6734.50	Shale	0.40048	30.94269	8.40927	1253.608	389.5536	11.48086	1849.14
6867.00	Sand	0.34907	38.18633	12.09349	2276.398	632.113	17.56936	2674.767
6900.00	Shale	0.36308	37.42426	11.66436	1977.059	562.6023	15.89326	2599.939
7019.00	Sand	0.34900	37.43645	11.46373	2149.319	610.2806	17.57717	2696.811
7038.00	Shale	0.38037	34.57135	10.13458	1595.095	474.1401	13.84253	2181.89
7063.50	Sand	0.35256	37.39647	11.52822	2134.824	603.4628	17.15018	2444.726
7115.50	Shale	0.39263	30.91798	8.46560	1399.904	425.1372	12.39981	1937.534
7235.00	Sand	0.35447	36.57107	11.03556	2035.576	583.3498	16.92129	2417.022
7273.00	Shale	0.37408	33.39162	9.52004	1673.777	495.3378	14.58662	2089.521
7318.50	Sand	0.37694	33.05543	9.36638	1621.598	482.6187	14.24858	1974.365
7355.50	Shale	0.39967	30.47465	8.24096	1284.152	396.2242	11.57565	1719.539
7385.00	Sand	0.35880	35.88647	10.69019	1945.997	562.1067	16.40361	2170.466
7424.50	Shale	0.38811	32.50296	9.15282	1463.891	441.6972	12.93122	1912.369

7475.00	Sand	0.35526	35.67548	10.58821	2014.989	578.6928	16.82731	2354.087
7511.00	Shale	0.35724	37.94252	11.84339	2034.656	580.1075	16.59032	2390.534
7543.00	Sand	0.35478	37.28574	11.38574	2026.984	581.4302	16.8847	2385.229
7617.50	Shale	0.37992	33.54253	9.62048	1598.063	475.2035	13.8965	2122.994
7640.00	Sand	0.33312	40.86358	13.21684	2503.315	692.8777	19.49688	2844.12
7701.00	Shale	0.35124	38.18505	11.84378	2111.731	600.9261	17.30856	2675.871
7859.50	Sand	0.34218	39.50859	12.51512	2295.018	644.5942	18.39936	2845.669
7940.50	Shale	0.36649	35.83652	10.73308	1846.518	535.4966	15.4869	2358.658
7975.50	Sand	0.34768	37.40668	11.43397	2170.549	615.6525	17.7368	2624.538
8020.00	Shale	0.37685	34.73826	10.17647	1634.06	485.062	14.25896	2285.118
8112.50	Sand	0.33629	39.63810	12.56775	2421.88	674.4227	19.11233	2966.137
8165.00	Shale	0.34256	41.11301	13.42521	2331.612	650.7347	18.35326	2967.916
8210.00	Sand	0.32732	42.01588	13.97880	2770.507	746.505	20.20358	3137.741
8337.00	Shale	0.36782	36.75686	11.27391	1854.851	535.3245	15.32877	2377.844
8374.50	Sand	0.33112	40.63020	13.12061	2558.096	705.0462	19.74028	3081.817
8423.50	Shale	0.32239	44.29977	15.15995	2811.226	760.6675	20.80709	3418.839
8571.00	Sand	0.33237	40.41697	13.01308	2542.383	700.3067	19.58811	3238.747
8596.00	Shale	0.33595	41.18528	13.43258	2446.505	679.2837	19.15379	3114.7
8636.00	Sand	0.32545	41.71561	13.65124	2680.92	733.9539	20.43245	3223.611
8722.50	Shale	0.36429	36.75512	11.16160	1880.629	544.1601	15.74894	2577.857
8771.50	Sand	0.31005	45.44176	15.79621	3136.43	833.6973	22.32762	3461.7
8881.00	Shale	0.34308	40.24888	12.89783	2282.496	641.3265	18.29066	3066.119
9024.00	Sand	0.32482	42.03418	13.82388	2696.785	737.5534	20.50906	3406.203
9157.00	Shale	0.34443	40.71294	13.16587	2274.839	638.4078	18.12775	2985.117
9273.00	Sand	0.31188	44.61250	15.23655	3038.402	814.4181	22.10084	3648.171
9370.00	Shale	0.34758	40.23691	12.91724	2200.828	621.3148	17.7485	2940.679
9453.00	Sand	0.31402	44.24839	15.05185	2992.413	803.4665	21.83671	3660.57
9512.00	Shale	0.31752	45.51252	15.74233	2900.299	782.8204	21.40543	3748.557
9561.50	Sand	0.30938	45.93180	15.97411	3106.692	829.6508	22.41068	3906.855
9642.00	Shale	0.32542	44.01343	14.91622	2688.234	735.2879	20.43558	3673.01
9707.00	Sand	0.29015	49.54438	18.10356	3704.466	959.5182	24.81516	4453.201

9845.00	Shale	0.32292	44.69456	15.32058	2778.747	754.5534	20.74254	3739.964
9890.00	Sand	0.28701	50.29839	18.50869	3781.477	977.2911	25.21292	4461.611

Table 4: Summary of Geomechanical Parameters by Lithology for Well D

Measured Depth (ft)	Rock Type (Lithology)	Poisson's Ratio	Dynamic Young Modulus (GPa)	Static Young Modulus (GPa)	Uniaxial Compressive Strength (Psi)	Cohesion Strength (Psi)	Friction Angle (Degrees)	Mohr-Coulomb failure criterion (Psi)
5122.50	Sand	0.4019	7.9079	29.7804	1236.4501	384.9296	26.0834	1544.5092
5155.50	Shale	0.4171	6.8567	27.2831	1033.1742	331.4764	24.5437	1407.4919
5210.50	Sand	0.3932	8.1891	30.4233	1360.0778	416.9657	26.9325	1703.1311
5218.50	Shale	0.3928	8.3569	30.8379	1364.8069	418.2480	26.9735	1725.0663
5265.50	Sand	0.3867	8.7581	31.7317	1460.2099	442.3752	27.5326	1782.1583
5288.00	Shale	0.4139	7.0905	27.8678	1071.6345	341.8986	24.8947	1486.1237
5328.50	Sand	0.4002	8.4486	30.5227	1346.2971	407.4228	25.7342	1607.8951
5354.00	Shale	0.4125	7.3535	28.4765	1093.4657	347.3984	25.0144	1511.1185
5421.00	Sand	0.3910	8.7619	31.7010	1401.0440	426.9304	27.1106	1726.0630
5462.50	Shale	0.4074	8.0956	30.2255	1159.0495	364.8780	25.5521	1543.8662
5477.50	Sand	0.3730	11.0781	36.6690	1688.7248	499.2438	28.7417	1877.1645
5506.50	Shale	0.4004	7.7180	29.3677	1253.0989	389.5699	26.2531	1677.7120
5563.50	Sand	0.3796	9.5648	33.3586	1607.4470	477.1361	28.0938	1957.9338
5579.00	Shale	0.4008	7.9733	29.9001	1257.4540	389.9727	26.1642	1827.9587
5788.00	Sand	0.3753	10.4866	35.3194	1661.0927	491.7119	28.5089	2153.3637
5871.00	Shale	0.4003	7.9094	29.7343	1263.2636	391.6185	26.2253	1677.3122
6001.50	Sand	0.3845	9.6063	33.5451	1501.5816	452.4013	27.7087	1907.3497
6013.50	Shale	0.3798	9.8069	34.0355	1568.6674	469.7265	28.1562	1990.1530
6110.00	Sand	0.3783	9.6203	33.5782	1605.2909	478.1534	28.2505	2004.8140
6154.50	Shale	0.4043	N/A	N/A	1203.8541	376.4197	25.8512	1723.0132
6250.50	Sand	0.3753	N/A	N/A	1645.9174	488.8346	28.5478	2084.8302
6266.00	Shale	0.3859	N/A	N/A	1475.5454	446.0785	27.5962	2004.2287
6343.50	Sand	0.3692	N/A	N/A	1754.7990	515.5411	29.0720	2206.1890

6374.50	Shale	0.3839	N/A	N/A	1511.5883	454.8451	27.7552	2033.3264
6444.50	Sand	0.3728	N/A	N/A	1697.7763	501.1117	28.7390	2145.0205
6468.00	Shale	0.3913	N/A	N/A	1401.1176	426.5987	27.0618	1957.7706
6557.50	Sand	0.3653	N/A	N/A	1829.9352	533.6225	29.3923	2249.0849
6582.00	Shale	0.3958	N/A	N/A	1323.1182	407.3871	26.6792	1885.7690
6683.50	Sand	0.3693	N/A	N/A	1763.1649	516.9839	29.0359	2237.8174
6725.00	Shale	0.3724	N/A	N/A	1706.2785	503.1773	28.7755	2330.3358
6844.00	Sand	0.3501	N/A	N/A	2176.0527	613.6880	30.5899	2634.5370
6876.50	Shale	0.3800	N/A	N/A	1589.5704	473.4874	28.0683	2131.8068
6920.50	Sand	0.3714	N/A	N/A	1716.1239	506.0616	28.8865	2178.3570
6946.00	Shale	0.3922	N/A	N/A	1384.1365	422.5280	26.9921	1968.4434
6990.00	Sand	0.3495	N/A	N/A	2144.2328	608.7882	30.6804	2519.8189

4.3 Comparative Analysis of the Log-Derived Geomechanical Properties of Wells A, B, C, and D

Table 5 presents the comparative ranges of the log-derived geomechanical properties for Wells A, B, C, and D and demonstrates considerable spatial variability in the elastic and strength characteristics of the formations. The ranges of Poisson's ratio, Young's modulus, uniaxial compressive strength (UCS), cohesion, friction angle, and Mohr–Coulomb failure criterion indicate that the mechanical behaviour of the formations varies both between wells and across different lithological intervals.

The Poisson's ratio ranges from 0.3014–0.4060 in Well A, 0.3177–0.4316 in Well B, 0.2870–0.4181 in Well C, and 0.3495–0.4171 in Well D. Well B records the highest maximum Poisson's ratio (0.4316), whereas Well C has the lowest minimum value (0.2870). The relatively higher Poisson's ratio observed in Well B suggests comparatively greater deformability of some of its formation intervals, while the lower values in Well C are associated with relatively stiffer elastic behaviour.

The Young's modulus results reveal substantial differences in formation stiffness. Static Young's modulus varies from 8.02–18.64 GPa in Well A, 5.05–12.02 GPa in Well B, 6.73 – 18.96 GPa in Well C, and 6.86–11.08 GPa in Well D. Similarly, dynamic Young's modulus ranges from 29.95–50.13 GPa in Well A, 22.56 – 38.40 GPa in Well B, 26.96–50.30 GPa in Well C, and 27.28 – 36.67 GPa in Well D. Wells A and C therefore contain the stiffest formation intervals, with Well C recording the highest maximum static and dynamic Young's modulus values. Well B exhibits the lowest minimum values for both elastic moduli, indicating the presence of comparatively less stiff intervals.

The strength parameters show a similar pattern. UCS ranges from 1190.98–3406.38 psi in Well A, 863.57–2883.59 psi in Well B, 1018.32–3781.48 psi in Well C, and 1033.17–2176.05 psi in Well D. Well C records the highest maximum UCS of 3781.48 psi, indicating the presence of highly competent formation intervals. Well B records the lowest minimum UCS (863.57 psi), suggesting comparatively weak intervals within the well. The cohesion values also demonstrate this contrast, with Well C reaching the highest maximum cohesion of 977.29 psi, compared with 888.71 psi in Well A, 779.66 psi in Well B, and 613.69 psi in Well D.

The friction angle ranges from 25.63–34.28° in Well A, 22.93–33.12° in Well B, 24.46–35.26° in Well C, and 24.54–30.68° in Well D. Well C again records the highest maximum value (35.26°), while Well B has the lowest minimum value (22.93°). The relatively higher friction angles in Wells A and C indicate greater resistance to shear deformation within their stronger intervals, whereas the lower values in Well B suggest comparatively lower shear resistance.

The Mohr–Coulomb failure criterion, which reflects the combined influence of cohesion, friction angle, and the applied normal stress, further demonstrates the variability in formation strength. The calculated values range from 1472.21 – 4250.41 psi in Well A, 626.04 – 2589.29 psi in Well B, 1430.51 – 4461.61 psi in Well C, and 1407.49 – 2634.54 psi in Well D. Well C records the highest maximum failure strength (4461.61 psi), followed by Well A (4250.41 psi), while Well B has the lowest minimum value (626.04 psi). This indicates that the strongest formation intervals occur predominantly in Wells C and A, whereas Well B contains intervals with comparatively lower resistance to failure.

Overall, Table 5 indicates that Well C contains the most mechanically competent individual intervals, as demonstrated by the highest maximum values of static and dynamic Young's modulus, UCS, cohesion, friction angle, and Mohr–Coulomb failure criterion. Well A also contains highly competent intervals and generally exhibits strong elastic and strength characteristics. Well B displays the lowest minimum values for several key properties and the highest maximum Poisson's ratio, indicating comparatively weaker and more deformable intervals. Well D generally exhibits intermediate-to-low strength ranges, although some intervals possess appreciable mechanical competence. The observed variability is consistent with differences in lithology and burial conditions across the wells, with stronger and stiffer intervals generally associated with sandstone-dominated formations. These variations are important for evaluating the spatial distribution of formation strength and for subsequent geomechanical and wellbore-stability assessment.

Table 5: Comparative Ranges of Log-Derived Geomechanical Properties for Wells A, B, C and D

Geomechanical Property	Well A	Well B	Well C	Well D
Poisson's Ratio (ν)	0.3014–0.4060	0.3177–0.4316	0.2870–0.4181	0.3495–0.4171
Static Young's Modulus (GPa)	8.0169–18.6396	5.0485–12.0226	6.7254–18.9616	6.8567–11.0781
Dynamic Young's Modulus (GPa)	29.9452–50.1345	22.5582–38.3970	26.9612–50.2984	27.2831–36.6690
UCS (psi)	1190.98–3406.38	863.57–2883.59	1018.32–3781.48	1033.17–2176.05
Cohesion (psi)	372.33–888.71	285.28–779.66	327.68–977.29	331.48–613.69
Friction Angle (°)	25.63–34.28	22.93–33.12	24.46–35.26	24.54–30.68
Mohr–Coulomb Failure Criterion (psi)	1472.21–4250.41	626.04–2589.29	1430.51–4461.61	1407.49–2634.54

4.4 Implications of the Log-Derived Geomechanical Characterization

The log-derived geomechanical properties provide useful insight into the spatial variability of formation mechanical behaviour within the onshore X Field. Variations in Poisson's ratio, static and dynamic Young's modulus, uniaxial compressive strength (UCS), cohesion, friction angle, and Mohr–Coulomb failure strength indicate that lithology and burial depth are important controls on the elastic and strength characteristics of the studied formations. Sandstone intervals generally exhibit lower Poisson's ratio, higher elastic moduli, greater UCS, higher cohesion, larger friction angles, and greater Mohr–Coulomb failure strength than adjacent shale units, indicating superior mechanical competence. Similar lithology-dependent behaviour has been widely reported in sedimentary basins (Aadnøy & Looyeh, 2019).

The estimated geomechanical properties show that shale-rich intervals are generally more deformable and mechanically weaker than the sandstone units. In contrast, the deeper sandstone intervals display higher elastic stiffness and greater resistance to compressive and shear failure, reflecting the effects of progressive compaction, porosity reduction, and diagenetic cementation commonly associated with increasing burial depth (Fjaer *et al*., 2021).

Comparison of the four wells reveals clear spatial variations in mechanical behaviour across the field. Well C records the highest maximum values for static and dynamic Young's modulus, UCS, cohesion, friction angle, and Mohr–Coulomb failure strength. Well D's comparatively lower maximum values likely reflect incomplete log coverage in this well rather than genuinely weaker formations at depth, and this should be treated as a data limitation rather than a firm geological conclusion. Well D's dataset contains gaps in sonic log coverage across several intervals and does not extend to the same depth as Wells A, B, and C; consequently, the reported ranges for Well D likely underrepresent the full mechanical strength of its formations and should be interpreted with this limitation in mind. Conversely, Well B generally records lower elastic stiffness and strength parameters and a comparatively higher Poisson's ratio, indicating weaker and more ductile formations. Well A displays relatively high dynamic stiffness and strength, while Well D exhibits intermediate to high maximum strength characteristics. These differences emphasize the importance of field-specific geomechanical characterization for evaluating reservoir heterogeneity and identifying mechanically competent intervals (Ekefre *et al.*, 2025).

The developed log-derived geomechanical property estimates provide a useful framework for evaluating the elastic and strength behaviour of reservoir formations and for identifying mechanically stronger and weaker intervals within the study area. The findings also establish a foundation for future investigations integrating laboratory measurements, pore-pressure estimation, in-situ stress modelling, fracture gradient prediction, and three-dimensional geomechanical modelling to achieve a more comprehensive understanding of reservoir geomechanics in the onshore Niger Delta (Ebong *et al.*, 2023b; Etim *et al.*, 2025).

5.0 Conclusion

This study presented a comparative log-derived geomechanical characterization of four wells in an onshore Niger Delta field using conventional wireline logs. Gamma ray, density, compressional sonic, shear sonic, resistivity, and caliper logs were integrated to estimate key elastic and strength properties, including Poisson's ratio, static and dynamic Young's modulus, uniaxial compressive strength (UCS), cohesion, friction angle, and Mohr–Coulomb failure strength using established empirical relationships.

The estimated geomechanical properties demonstrate that lithology and burial depth strongly influence the mechanical behaviour of the studied formations. Sandstone intervals generally exhibit lower Poisson's ratio, higher elastic moduli, greater UCS, cohesion, friction angles, and Mohr–Coulomb failure strength than adjacent shale units, indicating greater mechanical competence. The general increase in stiffness and strength with depth reflects progressive compaction and diagenetic cementation within the clastic sedimentary formations.

Comparative evaluation shows that Well C records the highest maximum values for several key elastic and strength parameters, including static and dynamic Young's modulus, UCS, cohesion, friction angle, and Mohr–Coulomb failure strength. In contrast, Well B generally exhibits lower ranges of stiffness and strength and the highest maximum Poisson's ratio, indicating comparatively less stiff and more deformable formation intervals. Wells A and D display intermediate characteristics, although locally strong intervals occur within both wells. It should be noted that gaps in log coverage and a shallower maximum depth in the Well D dataset limit direct comparison with Wells A, B, and C, and the reported Well D ranges should therefore be regarded as a conservative estimate of that well's true mechanical strength. These variations highlight the spatial and lithological heterogeneity of formation mechanical properties across the study area.

References

Aadnøy, B. S., & Looyeh, R. (2019). *Petroleum Rock Mechanics: Drilling Operations and Well Design* (2nd ed.). Gulf Professional Publishing.

Abijah, F. A., & Tse, A. C. (2016). Geomechanical evaluation of an onshore oil field in the Niger Delta, Nigeria. *IOSR Journal of Applied Geology and Geophysics, 4*(1), 99 – 111.

Adeoti, L., Alile, O. M., & Uchegbulam, O. (2009). Geophysical investigation of saline water intrusion into freshwater aquifers: A case study of Oniru, Lagos State, Nigeria. Scientific Research and Essays, 4(3), 248–259.

Akpan, A.S., Okeke, F.N., Obiora, D.N. George, N.J. (2021). Modelling and mapping hydrocarbon saturated sand reservoir using Poisson's impedance (PI) inversion: a case study of Bonna field, Niger Delta swamp depobelt, Nigeria. J Petrol Explor Prod Technol 11, 117–132 (2021). https://doi.org/10.1007/s13202-020-01027-8

Akpan, M. J., George, N. J., Ekanem, A. M., & Ekong, U. N. (2022a). Petrophysical appraisal and 3-D structural interpretation of reservoirs in an onshore Niger Delta field, Southeastern Nigeria. *International Journal of Energy and Water Resources, 9*, 89–101. https://-doi.org/10.1007/s42108-022-00218-9

Akpan, M. J., George, N. J., Ekanem, A. M., & Nathaniel, E. U. (2022b). Utilizing Probabilistic Neural Network for Reservoir Assessment: A Case Study from an Onshore Niger Delta Field. *Researchers Journal of Science and Technology*, *2*(3), 55 – 67. https://doi.org/10.83080/rejost.vol2no3.41

Asquith, G. & Krygowski, D. (2004) Basic Well Log Analysis. American Association of Petroleum Geologists (AAPG) Methods in Exploration Series, No. 16, 2004

Burke, K. C., Dessauvagie, I. F. J. & Whiteman, A. J. (1972). Geological History of the Benue Valley and adjacent areas In: Dessauvagie, T. F. J. & Whiteman, A. J. (Eds). African Geology, Ibadan University Press, Ibadan. 187 – 205.

Chang, C., Zoback, M. D., & Khaksar, A. (2006). *Empirical relations between rock strength and physical properties in sedimentary rocks*. Journal of Petroleum Science and Engineering, 51(3–4), 223–237. https://doi.org/10.1016/j.petrol.20-06.01.003

Davarpanah, S. M., Bar, N., Török, Á., Tarifard, A., & Vásárhelyi, B. (2020). Determination of Young's modulus and Poisson's ratio for intact stratified rocks and their relationship with uniaxial compressive strength. *Australian Geomechanics, 55*(4), 101 – 118.

Doust, H., & Omatsola, E. (1990). Niger Delta. In J. D. Edwards & P. A. Santogrossi (Eds.), Divergent/passive margin basins American Association of Petroleum Geologists. (AAPG) Memoir 48, pp. 201–238.

Eaton, B. A. (1975). The equation for geopressure prediction from well logs. *SPE Paper 5544*, Fall Meeting of the Society of Petroleum Engineers of AIME, Dallas, TX.

Ebong, S. T., Ekanem, A. M., & George, N. J. (2023a). Reservoir Characterisation Using Seismic Inversion Techniques for Mapping of Prospects. *Researchers Journal of Science and Technology*, *3*(1), 1–13. https://doi.org/10.83080/rejost.-vol3no1.43

Ebong, S. T., Ekanem, A. M. & George, N. J. (2023b). Fluid Prediction Through Lithological Analysis in 'M' Oil Field Niger Delta: Using Rock Physics Approach. Earth Sciences Malaysia, 7(1): 55 - 61.

Ekanem, A. M., George, N. J., Thomas, J. E. & Udo, I. G. (2024). Geophysical investigation of aquifer flow unit characteristics in northern parts of

Akwa Ibom State, Southern Nigeria. *Results in Earth Sciences*, 2, 100017, ISSN 2211-7148, https://doi.org/10.1016/j.rines.2024.100017.

Ekefre, A. E., George, N. J., Udoh, A. C., Harry, T. A., & Etim, C. E. (2025). Predictive Analysis of Sand Production and Flow Implications using Petrophysical-Geomechanical Properties: A case of "ANY" Field, Niger Delta. Researchers Journal of Science and Technology, 5(2), 54–73. https://doi.org/10.83080/rejost.-vol5no2.174

Ekong, S. U., George, N. J., Udoh, A. C., & Ekefre, A. E. (2025). Integrated Reservoir Characterization and Bypassed Hydrocarbon Evaluation for Optimized Recovery in 'UDEN' Field, Niger Delta, Nigeria. *Researchers Journal of Science and Technology*, *5*(7), 67–84. https://doi.org/10.83080/rejost-.vol5no7.227

Etim, C. E., Edet, B. N., Harry, T. A., & Ekefre, A. E. (2025). *Integrated Log-Derived Geomechanical Characterization and Sand Production Prediction for Sand Management in the EL Field, Niger Delta*. Researchers Journal of Science and Technology, 5(8), 31 – 65.

Evamy, B. O., Herembourne, J., Kameline, P., Knap, W. A., Molloy, F. A. and Rowlands, P. H. (1978). Hydrocarbon Habitat of Tertiary Niger Delta. *American Association of Petroleum Geologists Bulletin*, 62, 1 - 39.

Fjaer, E., Holt, R. M., Horsrud, P., & Raaen, A. M. (2021). *Petroleum Related Rock Mechanics* (3rd ed., Vol. 72). Elsevier.

George, N. J. (2021). Integrating hydrogeological and second-order geo-electric indices in groundwater vulnerability mapping: A case study of alluvial environments. *Appl Water Science,* 11, 123. https://doi.org/-10.1007/s-13201-021-01437-x

George, N.J., Ekanem, A.M., Thomas, J.E. & Harry, T. A. (2022). Modelling the effect of geo-matrix conduction on the bulk and pore water resistivity in hydrogeological sedimentary beddings. *Model. Earth Syst. Environ.* 8, 1335–1349. https://doi.org/-10.1007/s40808-021-01161-0

George, N.J., Agbasi, O.E., Umoh, A.J, Ekanem, A.M., Udosen, N. I., Thomas, J.E., Aka, M.U. & Ejepu, J.S. (2025). Enhanced contamination risk assessment for aquifer management using the geo-resistivity and DRASTIC model in alluvial settings, Cleaner Water, 3, 100060, https://doi.org/-10.1016/j.clwat-.2024.100060

Gercek, H. (2007). Poisson's ratio values for rocks. *International Journal of Rock Mechanics and Mining Sciences*, 44(1), 1 – 13. https://doi.org/10.1016/j.ijrmms-.2006.04.011

Horsfall, O.I., Akpan, M.J., & George, N.J. (2024) Reservoir characterization of GABO field in the niger delta basin using facies and petrophysical analyses, Results in Earth Horsfall Sciences, 2 https://doi.org/10.1016/j.rines.2024.100038

Knox, G.J. & Omatsola, E.M. (1989) Development of the Cenozoic Niger Delta in Terms of the "Escalator Regression" Model and Impact on Hydrocarbon Distribution. In: van der Linden, W.J.M., *et al.*, eds., Proceedings of KNGMG Symposium on Coastal Lowlands, Geology, Geotechnology, Kluwer Academic Publishers, Dordrecht, 181-202.

Lamorde, M., Somerville, J. M., & Hamilton, S. A. (2014). *Geomechanical Characterisation of Analogue Sandstones for the Yield Energy Approach to Prediction of Debris Production and Wellbore Stability.* SPE-172037-MS, Abu Dhabi International Petroleum Exhibition and Conference, Abu Dhabi, UAE, 10–13 November 2014. DOI: 10.2118/172037-MS

Larionov, V.V. (1969). Borehole Radiometry. Moscow, U.S.S.R: Nedra.

Lawson-Jack, O., Uko, E. D., Tamunobereton-Ari, I., & Alabraba, M. A. (2019). Geomechanical characterization of a reservoir in part of Niger Delta, Nigeria. *Asian Journal of Applied Science and Technology (AJAST), 3*(1), 10–30.

Murat, K.C. (1972) Stratigraphy and Paleogeography of the Cretaceous and Lower Tertiary in Southern Nigeria. In: Dessauvagie, T.F.J. and Whiteman, A.J., Eds., African Geology, University of Ibadan, 251-266.

Obianwu, V. George, N. & Udofia, K. (2011). Estimation of aquifer hydraulic conductivity and effective porosity distributions using laboratory measurements on core samples in the Niger Delta, Southern Nigeria. *International Review of Physics*, 5(1), 19-24.

Ogbuagu, K. M., Ehirim, C. N., & Dagogo, T. (2025). Geomechanical characterization of a clastic reservoir in parts of Niger Delta, Nigeria. *Discover Geoscience, 3*, Article 11. https://doi.org/10.1007/s44288-025-00119-4

Rider, M. H., & Kennedy, M. (2011). *The geological interpretation of well logs* (3rd ed.). Rider-French Consulting Ltd.

Short, K. C., & Stauble, A. J. (1967). Outline of geology of Niger Delta. American Association of Petroleum Geologists Bulletin, 51(5), 761–799. https://doi.org/10.1306/5D25C0CF-16C-1-11D7-8645000102C1865D

Rybacki, E., Reinicke, A., Meier, T., Makasi, M., & Dresen, G. (2015). What controls the mechanical properties of shale rocks? Part I: Strength and Young's modulus. Journal of *Petroleum Science and Engineering*, 135, 702–722. https://doi.org/10.1016/j.petrol.2015.10.028

Tuttle, M. L. W., Charpentier, R. R. and Brownfield, M. E. (1999). The Niger Delta Petroleum System: Niger Delta Province, Cameroon, and Equatorial Guinea, Africa.

Udosen, N. I. & George, N. J. (2018). Characterization of electrical anisotropy in North Yorkshire, England using square arrays and electrical resistivity tomography. *Geomech. Geophys. Geo-energ. Geo-resour.* 4, 215–233. https://doi.org/10.1007/s40948-018-0087-5

Udosen, N. I., Ekanem, A. M., & Thomas, J. E. (2024a). Geo-hydraulic characterization of a coastal aquifer system in South-eastern Nigeria with the inverse slope method. *Researchers Journal of Science and Technology*, *4*(1), 1–20. https://doi.org/10.83080/rejost.vol4no1.82

Udosen, N. I., Ekanem, A. M., & George, N.J. (2024b). Appraisal of flood-prone litho-stratigraphic units via geo electrical technology. *Malaysian Journal of Geosciences* (MJG), 8(1), 26 - 37.

Umoh, J. A., George, N. J., Ekanem, A. M., Thomas, J. E., & Emah, J. B. (2022). Approximate delineation of groundwater yield capacity and vulnerability via secondary geo-electric indices and rock-water interaction hydrodynamic coefficients in a coastal environment. *Researchers Journal of Science and Technology*, *2*(3), 28–54. https://doi.org/10.83080/rejost.vol2no3.40

Umoh, J.A., George, N.J., Ekanem, A.M. Emah, J.B (2025). Characterization of hydro-sand beds and their hydraulic flow units by integrating surface measurements and ground truth data in parts of the shorefront of Akwa Ibom State, Southern Nigeria. *Int J Energy Water Res* **9**, 13–29. https://doi.org/10.1007/s42108-022-00215-y

Zoback, M. D. (2010). *Reservoir Geomechanics*. Cambridge University Press, Cambridge.